Trends in Applied Spectroscopy
Vol. 9, 2012

Original Communication

The considerations regarding application of low resolution continuum source atomic absorption spectrometry for simultaneous multi-element determination

Dmitri A. Katskov*

Department of Chemistry, Faculty of science, Tshwane University of Technology, Pretoria 0001, South Africa

ABSTRACT

The methodology of simultaneous multi-element electrothermal atomic absorption spectrometry (SMET AAS) has been developed based on the pulse vaporization of samples in a fast heated tube atomizer, CCD detection of transitory radiation from continuum source within 210-410 nm wavelength range and calculation of absorption at the selected wavelengths. The calculation algorithm permits the visualization of absorption spectrum, provides background correction and modification of running absorbance with final temporal integration of the modified signals. This approach was verified using an Ocean Optics CCD spectrometer (1200 mm^{-1} groove density; 5 μm slit width; 3648 pixels (190-410 nm); 4 ms data collection time), xenon arc lamp and fast heated (10 K/ms) graphite tube atomizer. The measurements for number of elements were performed using single sampling. The data for 80 spectra were collected during pulse vaporization and processed in Excel. The results obtained for the multi-element solutions reveal an opportunity of simultaneous determination of individual analytes over a concentration range of 3-5 orders of magnitude with a limit of detection at μg/L level. The analysis for multiple elements including the sampling, measurements and calculations is performed in about 1-2 minutes. The instrument is simple and compact. The example of analysis of underground water shows that beside of the quantification of the analytes the absorption spectra obtained can be employed for the characterization of major molecular constituents of the samples.

KEYWORDS: electrothermal atomic absorption spectrometry, simultaneous determination, continuum source, low resolution CCD spectrometer

1. INTRODUCTION

Atomic Absorption Spectrometry (AAS) was once the leading technique for trace element determination. Over the last two decades, interest in AAS began to wane because of the outdated concept of linear source measurements and fast development of Optical Emission Spectrometry (OES) with an Inductively Coupled Plasma (ICP) excitation source. However, recent achievements in High Resolution Continuum Source (HR-CS) AAS show that the utility of AAS has not been yet fully investigated. AAS and OES have different advantages and limitations in analytical practice. Limits of detection (LOD) characteristic for various modifications of the OES and AAS instruments are given in Table 1. The comparison of LOD and other merits of the related instruments should help to outline possible direction in further development of atomic spectrometry suggested in this work.

Simultaneous determination of multiple elements including rare and refractive metals or non-metals within 3-4 orders of magnitude working range is

*KatskovDA@tut.ac.za

Table 1. Limits of detection for the commercial AA and ICP-OES instruments [1-3] and those measured in [8] and envisaged.

Element	Simultaneous ICP- OES (Varian Vista MPX)		Sequential linear spectrum source AA (Varian)				Continuum source AA				
							Sequential, Analytik Jena ContrAA 700, FWHM 2.7-6.7pm				Simul-taneous, FWHM 120pm
	Wavelength/nm	LOD Axial(radial) /µg/L	Wavelength/nm	LOD/µg/L		LOD(flame)/ LOD(furnace)	Wavelength/nm	LOD/ µg/L			
				Flame	Furnace[a]			Flame	Furnace[a], Estimation[c]	Furnace[a]	
										Prediction[d]	Measured[b] in [8]
Ag	328.068	0.5(1)	328.1	2	0.035	57	328.068	0.9	0.02	0.4	0.7
As	188.985	3(12)	193.7	300	0.5	600	193.696	350	0.6	27	
Bi			223.1	50	0.45	111	223.061	11	0.6	4	1.1
Cd	214.439(II)	0.2(0.5)	228.8	2	0.01	200	228.802	0.7	0.004	0.2	
Co	238.892(II)	0.4(1.2)	240.7	5	0.021	238	240.725	1.9	0.008	0.3	12
Cr	267.716(II)	0.5(1)	357.9	6	0.075	80	357.868	1.4	0.02	0.4	0.4
Cu	327.395	0.9(1.5)	324.7	4	0.03	133	324.754	0.6	0.005	0.1	4
Fe	238.204(II)	0.3(0.9)	248.3	6	0.06	100	248.327	1.7	0.02	0.6	2.1
Ga			294.4	100	0.22	455	287.427	25	0.06	1.7	
In			303.9	40	0.35	114	325.609	8	0.07	2	0.9
Mn	257.610(II)	0.1(0.2)	279.5	2	0.03	67	279.482	1.2	0.02	0.6	3
Ni	231.604(II)	0.7(2.1)	232.0	10	0.24	42	232.003	6	0.15	5.5	
Pb	220.353(II)	1.5(8)	217.0	10	0.27	37	217.001	12	0.3	13	0.9
Pt			265.9	100	0.35	286	265.945	28	0.1	3.3	
Sb	217.581	3(16)	217.6	40	0.5	80	217.581	23	0.3	12	
Se	196.026	4(16)	196.0	500	0.7	710	196.026	150	0.2	10	
Sn	189.93	2(8)	235.5	100	0.5	200	224.605	110	0.6	20	
Te	214.281	27	214.3	30	0.45	67	214.281	27	0.4	17	
Tl	276.787	16	276.8	20	0.75	27	276.787	7	0.3	8	0.1
Zn	213.856	0.2(0.8)	213.9	1.0	0.007	133	213.856	1.1	0.01	0.3	

[a,b]-20 and 10 µL injection, respectively
[c]-Estimated using LOD(flame) to LOD(furnace) ratio for linear source AAS
[d]-Predicted under the consideration that the determination sensitivity was inversely proportional to FWHM

possible using an ICP OES spectrometer equipped with a charge-coupled device (CCD) megapixel matrix, e.g. Varian Vista-MPX [1], or set of linear CCD detectors, e.g. Spectro Ciros [2]. This method provides a LOD of 0.1-10 µg/L and fast analysis times in a high-throughput laboratory. The limitation of the ICP OES originates from quantification of the analyte by atomic and ion emission lines excited in the plasma. High density of the lines in the ICP radiation spectrum require sufficient resolution of the spectral instrument (full width at half maximum (FWHM) of the transmittance profile less than 10 or 20 pm should be provided for the wavelength below 400 and 700 nm,

respectively [3]). The need for continuous dispersion of the sample solution in the ICP torch limits the concentration of the dissolved solids to less than 5% [1] and restricts the substances that can be analysed directly. The dependence of the output emission on the excitation conditions changes the sensitivity according to matrix composition. Finally, sample analysis using ICP OES can be costly due to the high consumption of Ar (10-12 L/min [2]).

There are reservations regarding the use of AAS due to the slow speed of traditional linear source AAS. However, important advantage of AAS for element determination is the small number of atomic absorption lines relative to the emission spectrum. According to the estimation by Lvov [4], “in AA due to smaller number and lower width of absorption lines the probability of their overlapping is in average by two orders of magnitude less than that for the respective emission spectra”. Respectively, FWHM of the transmittance profile of the monochromator about 0.2-2 nm is adequate for the AA measurements [5]. The AA spectrometer is employed either using continuous dispersion of the solution in the flame or with pulse atomization of dry sample residue in graphite tube atomizer (GTA). The sample in the atomizer can be modified by the added chemicals and by programmed thermal treatment, which together provides complete release of the analyte atoms during the atomization pulse. For a sampling volume of 20 µL the GTA provides an LOD on average of one hundred times lower than Flame atomization (Table 1) due to a longer residence time of atoms in the analytical volume and close to 100% efficiency in atoms production.

Recent progress in HR-CS AAS is associated with the instrument including an echelle monochromator (FWHM of the instrumental profile 2.7 pm at 200 nm and 6.7 nm at 500 nm) coupled to a linear detection system with a single continuum radiation source [6]. According to the concept of the sequential spectrometer, only a small spectral window (about 1 nm) is detectable simultaneously, but any wavelength position of the window is available within a broad wavelength range. The spectral window can be monitored with a high repetition rate using a 500 pixels CCD to detect pulse GTA absorption signals. Although a fast readjustment of the spectral window can be performed, various elements can be determined only sequentially. For pulse atomization signals the working range is limited, however, line wings, less sensitive lines or a special linearization algorithm can be employed to broaden the range [7]. The narrow spectral window and high light output of the continuum radiation source (Xe arc) elicit a lower LOD for flame HR-CS AAS in comparison to the traditional linear source AAS (Table 1). In general a one hundred fold reduced LOD can be expected for the GTA that makes it on average about 50 times more sensitive than ICP OES. Although HR-CS AAS with GTA surpasses ICP OES with regards to LOD for commonly determined elements and has more freedom from spectral and chemical interferences, it yields in the possibility of simultaneous multi-element determination. Similar to ICP OES, high spectral resolution increases instrument costs.

For simultaneous multi-element AA determination, a continuum spectrum of primary light within the 190-400 nm range is sufficient for analysis. For the instrument with linear CCD detection this working range can be obtained on account of the reduced spectral resolution. The reduction of resolution will cause reduction of absorbance magnitude and broadening of the lines. However, due to the relatively small number of absorption lines, their broadening up to some limit should not cause overlap. The sensitivity reduction can be compensated for by using furnace atomization. Thus, it is expected that a low resolution continuum source AA spectrometer coupled to GTA can provide simultaneous multi-element determination with a LOD similar to or lower than traditional single element Flame AAS (Table 1). The LOD can be further reduced on account of optimal GTA design, higher intensity of primary radiation, fast heating and repetitive injection of the solution or sampling of the slurry or solids.

The simultaneous multi-element electrothermal AAS (SMET AAS) analysis was first performed by Katskov and Khanye [8] using an instrument design described for the investigation of the molecular components of the vaporization spectra, e.g. [9-12] and new atomizer [13]. The calculation algorithm was initially developed and experimental problems were previously discussed in [8].

The instrument design and calculation method was later applied to the simultaneous determination of Al, Fe, Mn and Cu in coal slurry using a Filter Furnace atomizer [14]. These previous studies revealed the potential of the described method and provided the rationalization for modification of the instrument design and further investigation and development of the calculation software. The results of respective theoretical and experimental investigations are shown in this paper.

2. Theory

Pulse sample vaporization in the atomizer leads to the appearance of free atoms of the analyte in the absorption volume that cause absorption of radiation continuum from the primary light source within the atomic absorption line profile. For low vapor concentrations, the absorbance of the analyte at wavelength λ, is described by the following equation

$$A_t(\lambda) = \mathrm{Log}\,[I_0(\lambda)/I_t(\lambda)], \quad (1)$$

where $I_t(\lambda)$ and $I_0(\lambda)$ are radiation fluxes from the primary source passing through the atomizer with and without absorption, respectively. The respective absorption line is characterized by full width at half maximum (FWHM), $\delta\lambda_A$, which for the experimental conditions of ET AAS and various elements changes between 0.5 and 1.5 pm [7]. The concentration of atoms of the analytes in the absorption volume, n_t (mol·m^{-3}), is characterized by wavelength integrated absorbance, S_t (m), within the line profile,

$$n_t = (1/\gamma)\cdot S_t = (1/\gamma)\cdot \int_{\lambda} A_t(\lambda)\mathrm{d}\lambda, \quad (2)$$

where γ (m^4·mol) is coefficient, which characterizes the sensitivity of the absorption line, and the quantity of the analyte, N_0, fully released from the sample is characterized using temporal integration

$$N_0 = k\cdot \int_0^{\infty} n_t\,\mathrm{d}t \quad (3)$$

where k is the analyte vapor transportation rate, m^3/s (considered to be invariant towards mass of the analyte).

The realization of equation (2) in practice, however, meets limitations for the large concentrations of the analyte atoms in the gas phase. Atomic absorption in the atomizer is accompanied by resonance emission, which overlaps primary radiation passing through the atomizer. The contribution of emission causes distortion of the absorbance increasing with absorption magnitude:

$$A_t(\lambda) = \mathrm{Log}\{[I_0(\lambda)+I_{re}(\lambda)]/[I_t(\lambda)+I_{re}(\lambda)]\}, \quad (4)$$

where $I_{re}(\lambda)$ is flux of secondary resonance emission entering the spectrometer within the spatial angle determined by the geometry of the primary light beam through the atomizer and depending on the concentration of light absorbing species. In the tube atomizer of length (l) and internal diameter (d), in the absence of quenching processes, full absorption of primary radiation in the line center ($I_t(\lambda_0)$=0) should initiate emission signal from the center of the tube,

$$I_{re}(\lambda) = I_0(\lambda_0)\cdot d^2/(4\cdot l^2), \quad (5)$$

overlapping primary radiation. Substitution of (5) in (4) gives absorbance saturation level, which depends on the geometry of the tube and light beam. Eventually, absorbance in the line center reaches the saturation level A_s. Further increase of concentration of atomic vapor causes the spreading of the saturation beyond the line center.

The factors affecting the calibration curve within a broad vapor concentration range have been discussed previously [7]. It was suggested to approximate the absorption line profile by a triangle and trapezium for low and high concentrations of atomic vapor in the absorption volume, respectively. According to the model, high concentration of analyte atoms in the atomizer could be described by the following equation

$$n_t = (1/\gamma)\cdot(S_t + A_s\cdot\delta\lambda_A)^2/(4\cdot A_s\cdot\delta\lambda_A), \quad (6)$$

Atomic absorption is detected using a spectral instrument having a transmittance profile of $F(\lambda)$. The wavelength distribution of measured absorbance, $A'_t(\lambda)$ is determined by the convolution of the original line profile $A_t(\lambda)$ at given experimental conditions and instrumental transmittance profile [15],

$$A'_t(\lambda) = \int_{-\infty}^{\infty} F(\lambda')\,A_t(\lambda-\lambda')\mathrm{d}\lambda' \quad (7)$$

If FWHM of the instrumental profile, $\delta\lambda_F$, is much higher than that of the original absorption line, then

$$A'_t(\lambda) \cong F(\lambda)\cdot\int_{-\infty}^{\infty} A_t(\lambda)\mathrm{d}\lambda' = F(\lambda)\cdot S_t \qquad (8)$$

where wavelength integrated absorbance is invariant respective to the instrumental broadening of the line profile. For the triangle-type instrumental profile the measured absorbance in the line center is

$$A'_t(\lambda_0) = S_t/\delta\lambda_F, \qquad (9)$$

and, respectively,

$$n_t = (\delta\lambda_F/\gamma)\cdot A'_t(\lambda_0) \qquad (10)$$

or

$$n_t = (\delta\lambda_F/\gamma)\cdot(A'_t(\lambda_0) + C)^2/(4\cdot C), \qquad (11)$$

where

$$C = A_s\cdot\delta\lambda_A/\delta\lambda_F, \qquad (12)$$

for the low and high concentrations of analyte atoms in gas phase, respectively.

The combination of (10) and (11) provides general expression,

$$n_t = (\delta\lambda_F/\gamma)\cdot A^*_t, \qquad (13)$$

where

$$A^*_t = \{A'_t(\lambda_0) - 0.5[A'_t(\lambda_0) - (A'_t(\lambda_0) + C)^2/(4\cdot C)]\cdot[1+\mathrm{Sign}(A'_t(\lambda_0) - C)]\}, \qquad (14)$$

where Sign function is equal to -1 or 1 according to the sign of the argument.

The quantity of the analyte, N_0, fully released from the sample is characterized using temporal integration

$$N_0 = k\cdot\int_0^{\infty} n_t\,\mathrm{d}t \cong \delta\lambda_F\cdot(k/\gamma)\cdot\int_0^{tr} A^*_t\,\mathrm{d}t, \qquad (15)$$

where, t_r is registration time including the vaporization and transport processes.

For the instrument with CCD detection, the measurement results compose the data matrix where each value A (p, i) corresponds to the running absorbance A'_t (λ) integrated within the data acquisition time (τ) and averaged within the spectral interval of a single pixel. For the specific analyte, the set of A (p_a, i) data for the pixel p_a in the center of the absorption contour λ_0, approximates the temporal atomization profile. Quantities of various analytes in the sample can be found after modification of the data matrix,

$$N_{a0} = [\delta\lambda_F\cdot k_a\cdot\tau/\gamma_a]\cdot\sum_i A^*(p_a, i), \qquad (16)$$

where

$$A^*(p_a,i) = \{A(p_a,i) - 0.5\cdot\{A(p_a,i) - [A(p_a,i)+C_a]^2/(4\cdot C_a)\}\cdot\{1+\mathrm{Sign}(A(p_a,i) - C_a)\}, \qquad (17)$$

if coefficients k_a/γ_a and $k_a/(\gamma_a\cdot C_a)$ for a particular analyte are known from independent calibration measurements.

The contribution of equation (10) and (11) in the general formulas (15) or (16) depends on the ability of the atomizer to create a high concentration of atomic vapor, spectral resolution of the instrument and output of the light source at specific wavelength. It can be roughly evaluated taking into account the data on $A_s\cdot\delta\lambda_A$ parameter reported previously in [7] for the HR-CS instrument. According to the estimations [7], $\delta\lambda_A$ e.g., for Pb 283.31 nm absorption line varies between 0.75 and 0.64 pm for temperatures 2800 and 2400 K, respectively, while the measured $A_s\cdot\delta\lambda_A$ parameter is close to 0.6 pm. Respectively, the saturation level A_s can be found equal to about 0.8-0.9. For the low resolution instrument, this value is reduced according to $\delta\lambda_A$ to $\delta\lambda_F$ ratio [15]. Thus, for the instrument [8] having FWHM of the transmittance profile about 0.15 nm, absorbance, A'_s should be equal to 0.001-0.002. If the absorbance corresponding to the LOD exceeds this limit, formula (17) is substantially simplified to,

$$A^*(p_a,i) \cong [A(p_a,i)]^2/(4\cdot C_a). \qquad (18)$$

Finally, quantity of the analyte can be found,

$$N_{0a} = [\delta\lambda_F^2\cdot k_a\cdot\tau/(4\cdot\gamma_a\cdot A_s\cdot\delta\lambda_A)]\cdot\sum_i[A(p_a,i)]^2. \qquad (19)$$

In the following text the values corresponding to $\sum_i[A(p_a,i)]^2$ are called integrated modified absorbance.

For the instrument having higher spectral resolution the sensitivity increase is accompanied by rise of contribution of a linear part of the $A^*(p_a,i)$ vs $n_{t,a}$ function.

The absorbance calculation according to (1) considers two runs of temperature program, with and without sampling. The evolution of sample vapor can cause superposition of molecular absorption bands over the atomic lines. In this case, the wavelengths on distance $\Delta\lambda$ from the center of the absorption line can be employed for the background (BG) correction. Respectively, for the CCD instrument providing wavelength range $\Delta\lambda_p$ per pixel the BG corrected absorbance

$$\bar{A}\,(p_a,\theta,i) = A(p_a,i) - A(p_a\pm\theta,i), \qquad (20)$$

where $A(p_a\pm\theta,i)$ is equal to average of $A(p_a+\theta,i)$ and $A\,(p_a-\theta,i)$, for θ equal to $\Delta\lambda/\Delta\lambda_p$. Thus, $\bar{A}(p_a,\theta,i)$, instead of $A(p_a,i)$, will compose the data matrix and, respectively, quantity of the analyte can be found,

$$N_{0a} = (1/\alpha_a)\cdot\sum_i [\bar{A}\,(p_a,\theta,i)]^2, \qquad (21)$$

where, general sensitivity coefficient α_a (1/mol), according to (19), depends on multiple parameters including the characteristics of the spectral line, mass transfer of the analyte, design of the atomizer and data acquisition rate. In the text below the values corresponding to $\sum_i [\bar{A}\,(p_a,\theta,i)]^2$ are called integrated BG corrected modified absorbance.

For low concentrations of the analyte, while the line contour is fully located within the range of $p_a\pm\theta$ pixels, $\bar{A}\,(p_a,\theta,i)$ is equal to $A\,(p_a,i)$ and, respectively, the linearization algorithm (18) can be applied to the data matrix. Too broad a $p_a\pm\theta$ range can include absorption lines in addition to the analyte metals potentially contributing to spectral interference. On the other hand, the choice of narrow $p_a\pm\theta$ range within the line contour will reduce sensitivity and make the linearization algorithm (18) less effective. If the data matrix includes several absorption lines for a particular analyte, the lines less prone to interference, as well as optimal $p_a\pm\theta$ range, can be selected from the overview of spectrum $\sum_i A(p_a, i)$.

3. EXPERIMENT

The aim of the experiment was to verify the quantitative simultaneous atomic absorption determination of a group of elements, detect limitations in the hardware and software, outline the analytical performance of the prototype instrument and suggest prospects for further development of AA methodology.

3.1. Setup

The diagram of the experimental setup and visualization of the measurement concept is reported in Figure 1. The spectrometer was Ocean Optics model HR4000 [16]. The grating 1200 grooves per mm and 5 µm spectral slit provided FWHM about 120 pm within 190-410 nm wavelength range. The radiation spectrum was registered using Toshiba 3680 pixels CCD and the Spectra Suite software, which provided minimum acquisition time for a single spectrum 4 ms.

The Xe arc (L 2174, 75 W, Hamamatsu) [17] provided the continuum light source. Radiation from the lamp was focused by two lenses into the center of the graphite tube atomizer and on the entrance slit of the spectrometer. Because of the high intensity of light above 220 nm, attenuation was required even with a short, 4 ms, acquisition time to avoid saturation of the CCD. The attenuation made impossible the absorption measurements near and below 210 nm. Although a less intense deuterium lamp could support the measurements below 210 nm [8], in this work only Xe arc was employed in order to facilitate frequent data acquisition and a relatively low LOD.

The vaporization unit with power supply had been specially built for the experimental setup by Cortec (Moscow, Russia) [18]. The design of the unit and power supply provided programmed heating, fast ramp (10°C per ms), and stabilization of temperature of the tube during the atomization stage. Graphite tubes designed according to our specifications were manufactured by Schunk (Germany). The size and configuration of the longitudinally heated tube allowed for a ring shaped carbon fiber (Alfa Aesar, USA) collector in the center. The amount of carbon fiber was adjustable or the tube used without a collector. The sampling hole was reduced to 1.2 mm for the nozzle (Greiner Bio-One, Germany) to inject the sample solution. The characteristics of the atomizer were previously discussed [13]. A new addition to the setup was a bubbler containing CCl_4 to clean the tube after several measurements. During the

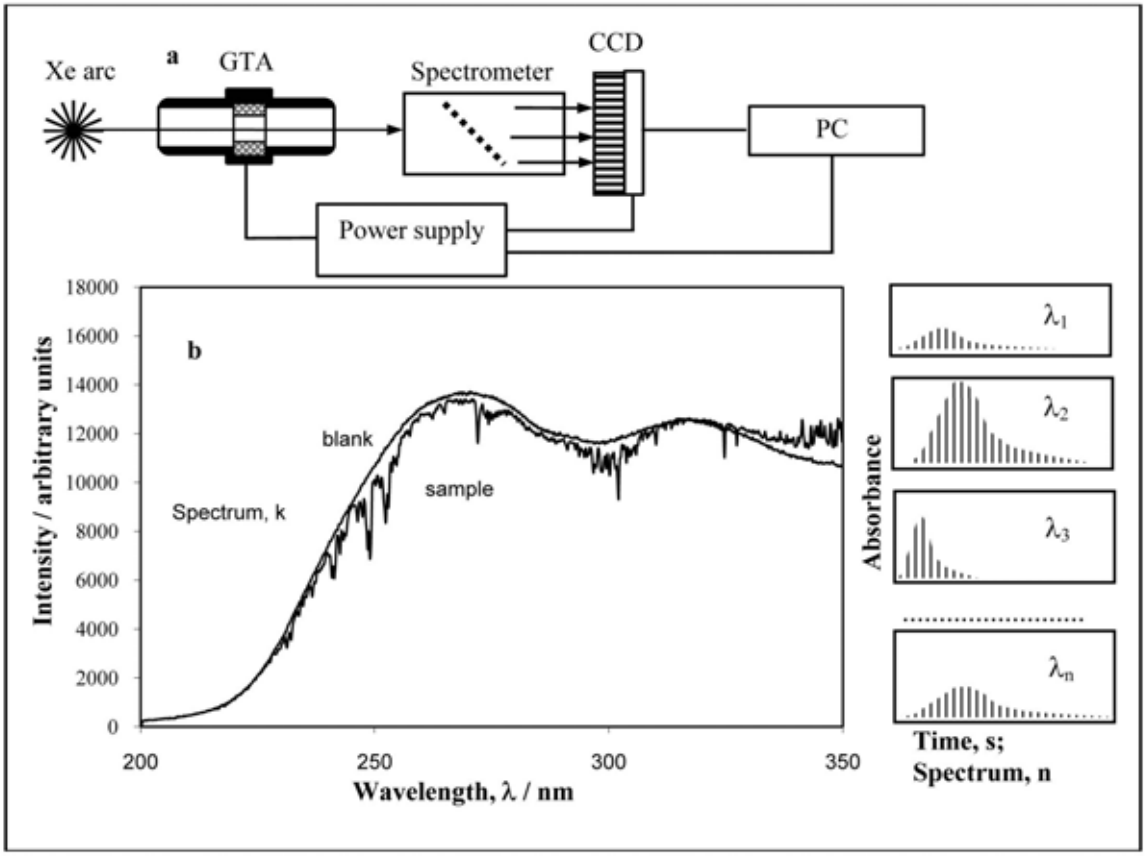

Figure 1. Experimental setup (a) and visualization of the measuring principle (b).

cleaning program, Ar flow (about 0.5 L/min) was directed to the tube ends through the bubbler.

3.2. Samples

The elements Al, Ca, Cd, Co, Cu, Cr, Fe, Mg, Mn, Ni, Pb that are each frequently determined in environmental research were selected for experiments in this study. The spectra of these elements were investigated; most sensitive analytical lines selected and calibration curves built using the sets of solutions prepared from 1000 mg/L reference solutions (Merck, South Africa) by sequential 5 fold dilutions with de-ionized water containing 0.2% of nitric acid. The results were compared with the data for the solutions prepared by sequential 2 fold dilutions of multi-element reference material (Spectrascan, Industrial Analytical, South Africa) containing 0.5±0.003 µg/L of Al, As, Cd, Co, Cr, Cu, Fe, Mn, Ni, Pb, V and Zn in 2% HNO_3 (in the text it is referred to as Mixture 1). The determination methodology was also verified using the 0.5 mg/L solution of Al, As, B, Ba, Be, Bi, Ca, Cd, Ce, Co, Cr, Cs, Cu, Fe, In, K, Li, Mg, Mn, Na, Ni, Pb, Rb, Se, Sr, Tl, U, V, Zn prepared from the stock 100±0.5 mg/L in 5% HNO_3 reference material (Spectrascan) by dilution with water (Mixture 2) and 0.5 mg/L solution in water of Al, B, Cr, Co, Cu, Fe, K, Mg, Mn, Na,Ni, P, Pb, Si, Sn, Ti, V, Zn prepared from the stock reference material for ICP OES spectrometry (50 mg/L in 4.9% HCl with trace HF) (Mixture 3).

Five samples of underground borehole water (referred to in the text as BH (1-5)) collected from locations around Pretoria, South Africa were used to reveal potential problems related to practical applications of the instrument. The injection volume 10 µL was used for all the samples and reference solutions.

3.3. Procedure

The light source, power supply of the atomizer and computer were switched on and mutual

positions of the components of optical arrangement were adjusted to provide maximum CCD output in the shorter wavelength area. Next, the program was set for measurement or alternative cleaning. The measurement program included the drying, pyrolysis, atomization and cleaning steps with normal Ar flows (Table 2). Similar temperature ramp from initial (500°C) to final (2600°C) temperature at the atomization step was used for all measurements that provided full release of atomic vapor with gas-stop mode during 1-1.5 s. The program for alternative cleaning included five 1s maximum power heating pulses to 2000°C, during which Ar flow was directed to the tube ends through the bubbler. After the cleaning, initial blank ran of the temperature program with data acquisition, calculation and visualization of the blank absorption spectrum was performed to evaluate the cleaning results. If there were no outstanding absorption lines in the blank spectrum, subsequent measurements were performed.

The Ocean Optics software, beyond the direct data acquisition, provided an option with averaging of the CCD outputs for certain number of sequential acquisitions. At this stage of research total number of spectra acquired within 4 ms or as an average within 8 or 12 ms (for slower absorption pulses) was limited by 80. The data files were opened in Excel as tables of the CCD outputs. Maximal size of each $I(p,i)$ Excel table was 3680×80 cells (190-410 nm wavelength range and 80 spectra obtained). Of that 18×80 of the Excel cells were used for automatic correction of dark current.

The $I(p,i)$ and $I_0(p,i)$ values obtained with and without sampling were used for calculation of absorbance $A\ (p,\ i)$. Respective matrix permitted the visualization of the spectrum for particular time t from the beginning of the atomization stage, $A\ (p,\ i=t/\Delta t)$ (Δt is full time for data acquisition and transfer including spectra averaging) or integrated spectrum $\sum_i A(p,\ i)$, as well as temporal changes of absorption at particular wavelength. The matrix of BG corrected and modified data $[\bar{A}\ (p_a,\theta,i)]^2$ was obtained using pixel number θ equal to 2, 3 or 4. The integrated values $\sum_i [\bar{A}\ (p_a,\theta,i)]^2$ were automatically calculated for various lines and presented in special table. The calculation time from data transfer to final result took only several seconds independent of number of lines. The temporary integrated absorption spectra and BG corrected modified absorbance spectra signals were plotted and, if necessary, parameters θ and i changed to obtain better BG correction or LOD.

The examples, which illustrate main characteristics of the setup, are shown in Figures 2 and 3. The contour of temporally integrated absorbance spectrum in Figure 2 observed during pulse atomization of Mn (12 μg/L) shows absorption triplet (279.482, 279.827 and 280.108 nm). The components of the triplet are about 50 times broader in comparison with respective spectrum in the flame HR-CS instrument [6]. The integrated absorption spectrum for high concentration of Al (40 mg/L) in the injected solution without and with BG correction (using pixels p_a±3) is shown

Table 2. Temperature programs.

Program	step	Temperature /°C	Ramp time/s	Hold time/s	Internal gas, flow rate/ L/min
Measurements	drying	110	5	10	Ar, 5
	pyrolysis	500-800	5	10	
	cooling	500		2	Gas stop
	atomization	2600	0[a]	3	
	cleaning	2600	0[a]	1s × 5[b]	Ar, 5
Alternative cleaning		2000	0[a]	1s × 5[b]	Ar; CCl_4, 0.5[c]

[a]-maximum power heating
[b]-5 maximum power pulses with 1s interval
[c]-Ar supplied through the bubbler filled with CCl_4

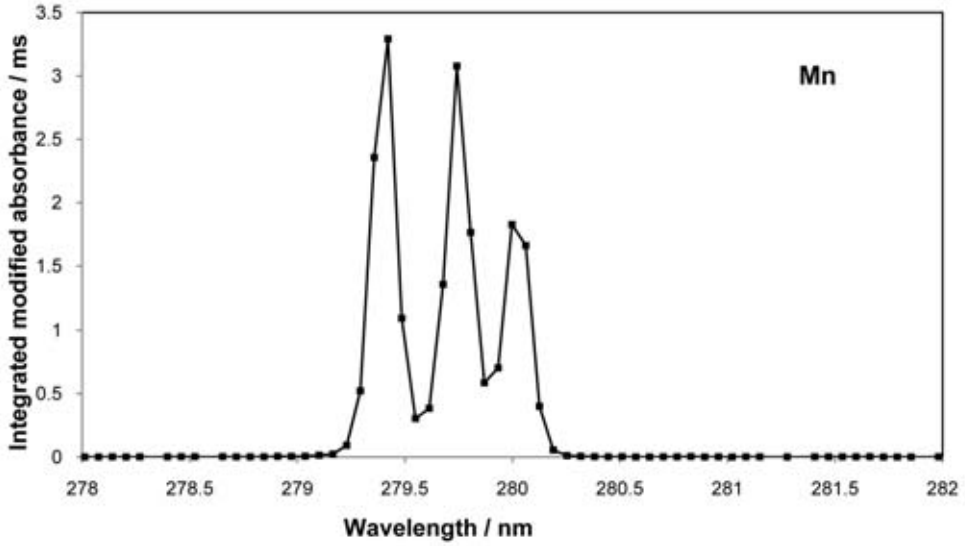

Figure 2. Integrated modified absorption for the solution 12 μg L^{-1} of Mn at 179.482, 279.827 and 280.108 nm.

in Figure 3, a and b, respectively. It is seen that the bands with maximums at about 254 and 214 nm have been removed from the BG corrected modified spectrum together with absorption continuum.

4. RESULTS AND DISCUSSION

4.1. The measurement problems

4.1.1. Stability of the wavelength calibration and correction

The wavelength calibration of the spectrometer was performed using the absorption lines of several elements that resulted in the approximation of wavelength (λ vs. pixel number (p) by function $\lambda = -0.00000123773 \cdot p^2 + 0.0674013 \cdot p + 190.237$ nm with correlation coefficient $R^2 = 0.9999$. Since $\lambda(p)$ function was almost linear, the averaged spectral interval about 0.055 nm could be attributed to single pixel. Taking into account FWHM of the instrumental transmittance profile (0.12 nm) and considering it as a triangle, it can be concluded that the atomic line should occupy about 5 pixels. The estimation gives an approach to the selection of pixels $p_a \pm 3$ to be used for the background correction.

It was uncovered in the course of experiments that some uncontrollable factors (e.g. outward temperature or adjustment of the light source) could cause a shift in the absorption maximum vs. pixel number. Normally, the shift did not exceed ±1 pixel. Since the nature of the error source was unclear, there was no chance to stabilize the λ to p ratio on account of experimental conditions. It was suggested, instead of using a fixed for each line pixel number, to select automatically the maximum from the data of 5 pixels around each absorption line. The respective option was included in the calculation program and was applied to all data shown in this study.

4.1.2. Memory effects and cleaning of the atomizer

One of the problems related to the use of the longitudinally heated atomizer for multi-element determination was condensation of less volatile components of sample vapor next to the cooled ends. If the condensation occurred, the subsequent blank run of temperature program was accompanied by incipient spectrum of the deposited metals. The design and operation of longitudinally heated tube atomizer [13] employed in this work made possible efficient reduction of sample memory on account of predominant heating of the tube ends during the cleaning stage by maximum power electrical pulses and vapor removal based on venturi effect. However, the removal of deposits associated with excessive amounts of low volatile substances required multiple repetitions of the temperature program that caused premature damage of the tube ends.

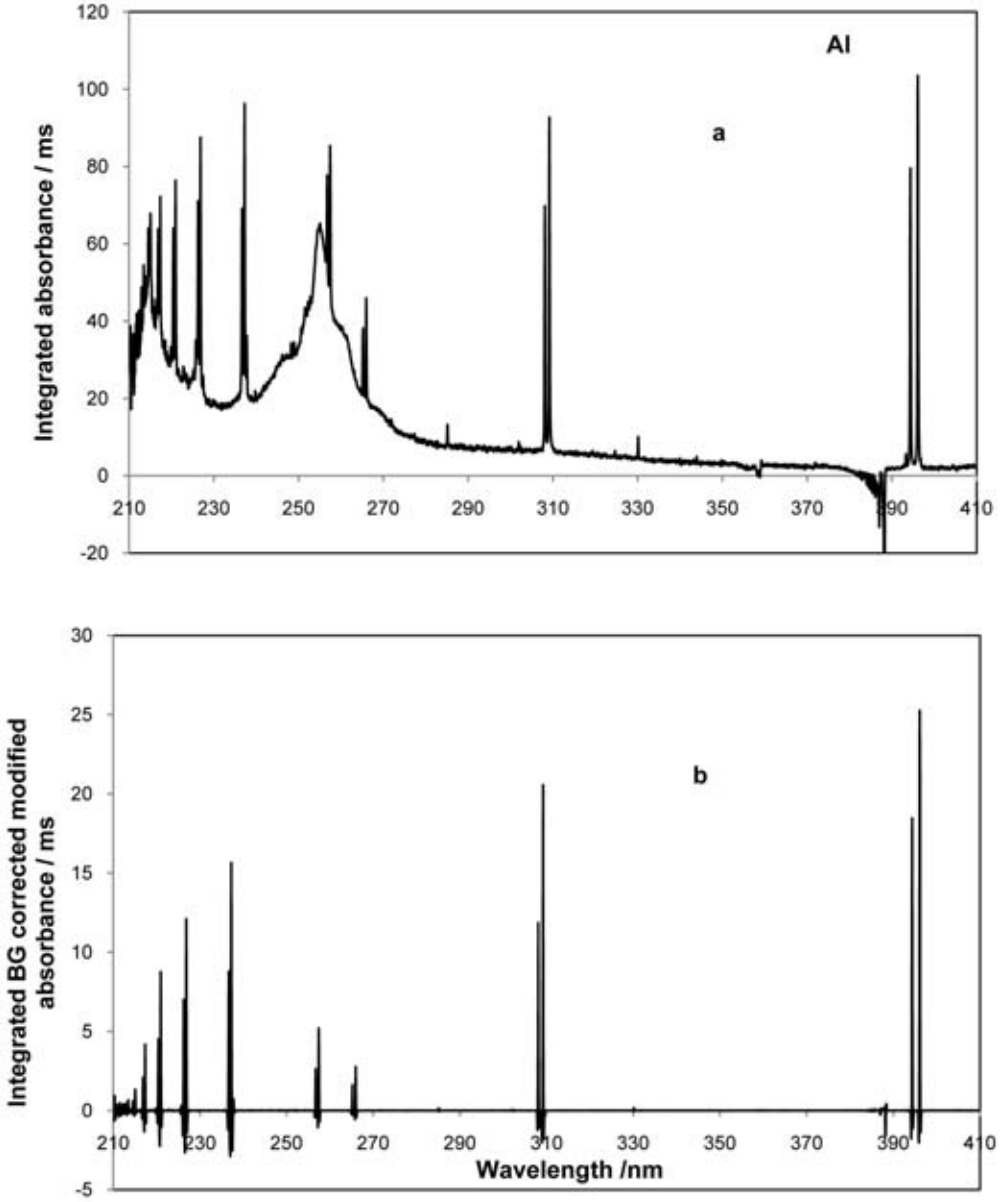

Figure 3. Integrated absorption spectrum for the solution 40 mg L^{-1} of Al: original (a) and after the BG correction and modification (b).

Effective chemical cleaning of the atomizer was achieved when Ar saturated with CCl_4 was employed as a substitute for Ar in the ends flow during the run of temperature program (Table 2). The decomposition of the CCl_4 vapor at high temperature caused evolution of chlorine and, respectively, formation of volatile compounds with the metals deposited near the tube ends. After one or two runs of temperature program a complete reduction of memory signals was observed. One or two consequent blank runs of temperature program released the chlorine from the tube.

4.2. Absorption spectra of individual elements and their mixtures

The observed absorption spectra of individual elements consisted mainly of atomic lines; however, in some cases the molecular bands belonging to dimers, gaseous oxides or carbon containing

molecules could be present for the samples with high analyte concentrations. For example, the combination of atomic lines and molecular bands in vapor spectrum of Al is presented in Figure 3a. The persistence of a molecular band at 250-270 nm was attributed to Al_2O [19]. These molecular bands are removed from the spectra after BG correction (Figure 3b).

Of the elements selected for investigation Co, Ni and Fe have the richest atomic absorption spectra (Figure 4a, b and c). Besides resonance lines, some of the observed intense lines belong to the transitions from low excited levels. Other elements have a simpler absorption spectrum consisting of 1, 2, or roughly 3 lines. The most sensitive lines of several elements selected for the investigation

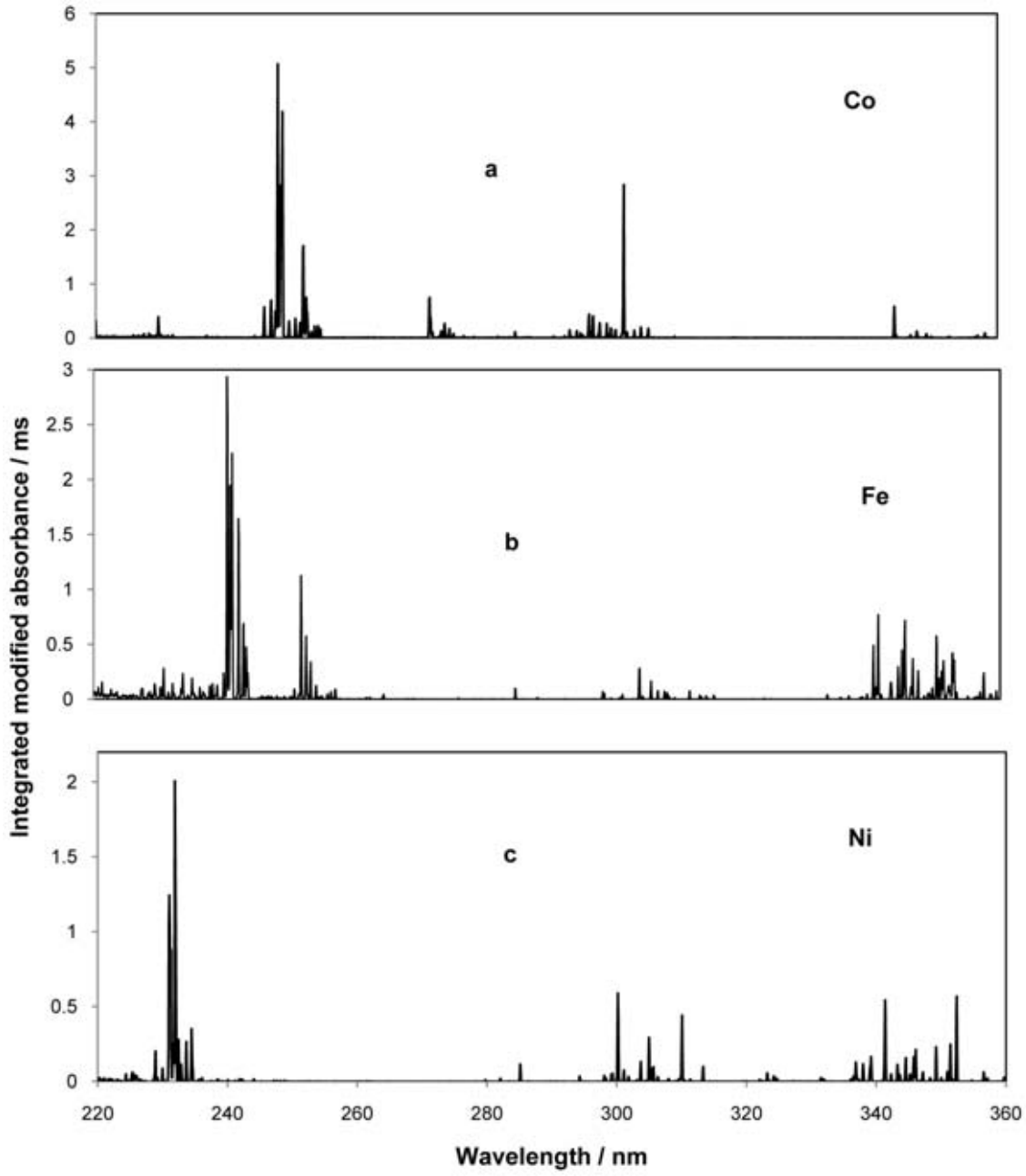

Figure 4. Absorption spectra for the single element solutions, 8 mg L^{-1}: a - Co, b - Fe, c - Ni.

Table 3. The approximations of the calibration curves for the single-element solutions in the GTA without carbon fiber collector.

Element, line		Range/ mg L^{-1}	Approximation			
			$\mathrm{LOG}\sum_i [A(p_a,\theta=3,i)]^2 = a\cdot \mathrm{LOG}\ M + b$			
			a	-b	R^2	LOD/ mg L^{-1}
Al	396.152	40-0.00256	0.977	0.307	0.999	0.003
	394.401	40-0.00256	0.987	0.592	0.988	0.005
	309.271	40-0.00256	0.915	0.503	0.996	0.005
	308.215	200-0.0128	0.924	0.787	0.996	0.013
	237.312	40-0.0128	0.973	0.645	0.988	0.016
Ca	239.55	200-0.064	0.992	1.081	0.998	0.053
	227.546	200-0.064	0.979	0.756	0.999	0.035
Cd	228.802	40-0.00256	0.887	-0.14	0.995	<0.001
Co	345.35	40-0.0128	0.808	1.18	0.992	0.044
	340.512	40-0.0128	0.867	1.286	0.992	0.041
	252.136	40-0.0128	0.871	0.822	0.999	0.017
	242.493	40-0.0128	0.837	0.713	0.996	0.015
	241.446	40-0.0128	0.812	0.876	0.998	0.033
	241.162	40-0.0128	0.815	0.931	0.999	0.043
	240.725	40-0.0128	0.844	0.503	0.999	0.009
Cr	360.532	40-0.00256	0.934	0.402	0.999	0.005
	359.348	40-0.00256	0.888	0.289	0.998	0.003
	357.868	40-0.00256	0.909	0.221	0.993	0.003
Cu	327.39	200-0.00256	0.855	0.374	0.999	0.003
	324.754	40-0.00256	0.862	0.025	0.999	0.003
Fe	302.064	40- 0.0128	0.818	0.537	0.996	0.006
	271.903	200-0.0128	0.772	1.343	0.999	0.066
	252.285	200-0.0128	0.802	0.808	0.998	0.016
	249.064	40-0.0128	0.847	0.758	0.995	0.018
	248.321	40-0.0128	0.865	0.362	0.998	0.007
Mg	285.213	8-0.00256	0.821	-0.880	0.999	<0.001
Mn	279.482	40-0.0128	0.862	-0.057	0.998	0.002
Na	330.237	200-1.6	0.71	0.063	0.98	0.005
	285.281	200-1.6	0.788	0.68	0.971	0.023
Ni	352.454	200-0.0128	0.821	1.179	0.998	0.029
	341.476	200-0.0128	0.85	1.233	0.995	0.031
	310.155	200-0.0128	0.859	1.309	0.997	0.021
	305.082	200-0.064	0.814	1.395	0.999	0.085
	300.249	200-0.0128	0.879	1.238	0.999	0.036
	232.003	200-0.32	0.931	0.886	0.999	0.040
Pb	283.306	40-0.0128	0.953	0.76	0.998	0.009

are listed in Table 3 where the wavelengths are indicated according to the reference data [20].

The integrated modified absorbance spectra for the mixed solutions corresponded to the superposition of the constituent of atomic spectra. The temporarily integrated absorption spectra in the tube without collector, obtained for the Mixtures 1-3 are shown in Figure 5, diagrams b, a and c, respectively. In Figure 5, the absorption spectra except the Mg 285 nm line are shown in similar scale. The rich spectrum for Mixture 2 includes In, Bi and Be lines. The molecular band at about 261 nm in the spectrum c belongs to AlCl [6], formed due to presence of HCl in the reference material. The BG correction shown in Figure 6 for the modified absorption spectrum stabilizes the zero line and reduces AlCl band, however, not completely because of the pronounced band head.

4.3. Absorption signals

It was shown previously that the carbon fiber collector in the tube provided a temporal shift of the sample vaporization and consequently a higher temperature of the analyte vapor in the absorption volume [13]. The presence of the collector in the atomizer provided a high degree of atomization of volatile sample components. However, the shift of the atomization pulse was accompanied by a reduction of peak magnitude that deteriorated the LOD. This observation is illustrated in Figure 7, where the absorption pulses are compared for nitrates (solid lines) and chlorides (dotted lines) from Mixtures 1 and 3 in the tube either containing or lacking the carbon

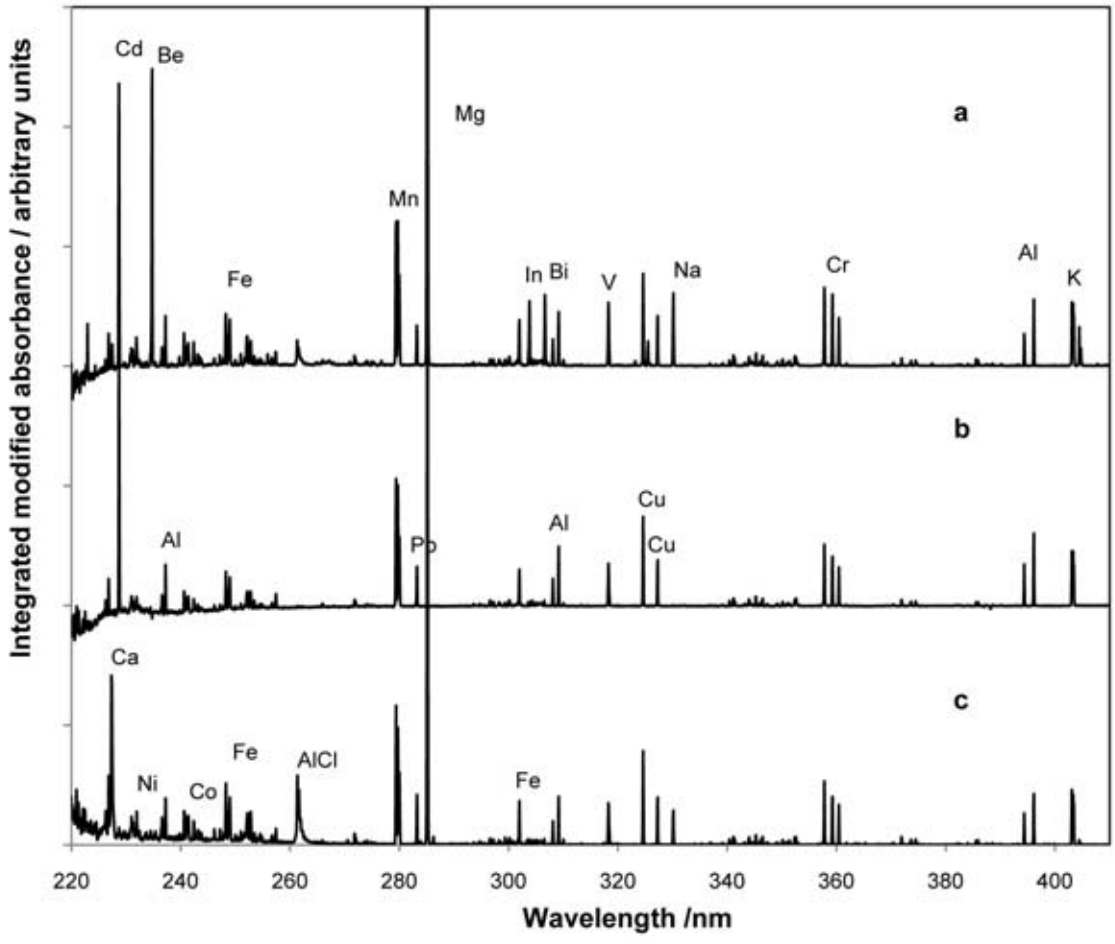

Figure 5. Integrated modified absorption spectra for the multi-element solutions, 0.5 mg L^{-1}, of each metal: a - Mixture 2, b- Mixture 1, c- Mixture 3.

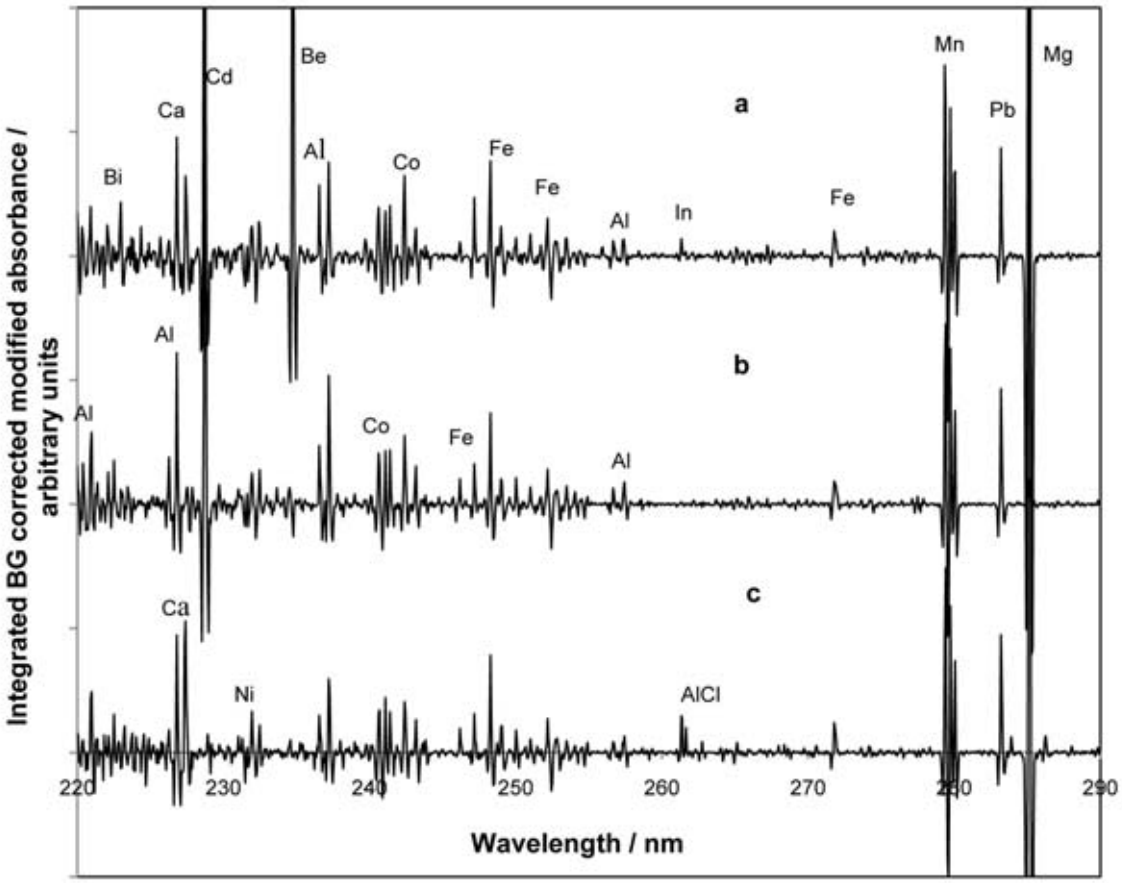

Figure 6. The parts of the integrated BG corrected modified absorption spectra for multi-element solutions, 0.5 mg L^{-1}, of each metal: a - Mixture 2, b- Mixture 1, c- Mixture 3.

fiber collector. For the majority of elements, the exception being Cu, the shift due to the collector is accompanied by a reduction of peak magnitude. In the case of V, the peak became hardly distinguishable from background. Cr and V share a tendency to form solid stable carbides, and the collector provided an adsorptive surface that reduced the concentration of the analyte in the vapor. For the majority of elements investigated in this work, except Al, the signals for the chlorides remained similar to those for nitrates independent of the presence of the collector. An absence of chemical interferences in the tube without the collector is likely due to the specific distribution of temperature along the tube during pulse heating (the ends are hotter than the center) [13], or a relatively high probability of collision of molecular species with the wall due to the narrow diameter of the tube atomizer (2.5 mm) compared to commercially available atomizers (5-6 mm). Indeed, the effect of tube diameter on chemical interferences in ET AAS is important and requires further investigation that is beyond the scope of this work. For now, however, it can be provisionally concluded that the carbon fiber collector is dispensable for the simultaneous determination of less volatile or carbide forming elements.

4.4. Calibration curves

It is proposed in the theory that after the squaring and integration of the running absorbance, which is not affected by BG, the calibration curves $\sum_i [A(p_a,i)]^2$ vs. m_a, concentration of the analyte in the sample, are to be approximated by straight lines with the slope depending on combination of coefficients in (19). Within broad concentration range in Log-Log coordinates it could be

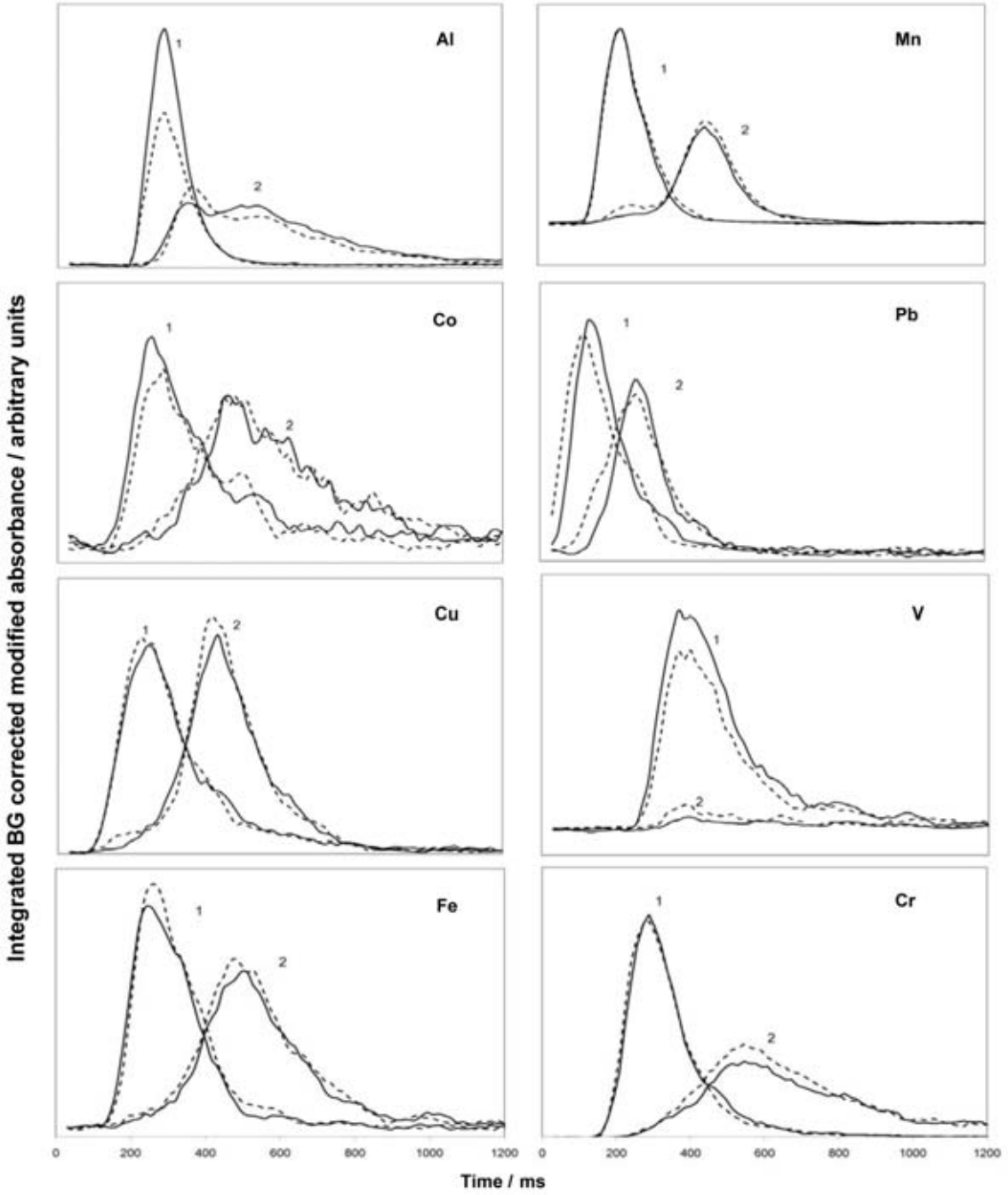

Figure 7. BG corrected modified absorption peaks for metals in multi-element solutions Mixture1 (solid line) and Mixture 2 (dotted line), 0.5 mg L^{-1} of each metal. 1, 2 in a GTA without and with carbon fiber collector, respectively.

presented by linear regression with the slope equal to unity. Unfortunately, this ideal option can hardly be realized in practice for the function $\mathrm{Log}\sum_i [\bar{A}\ (p_a, \theta, i)]^2$ vs. Log m_a, which is employed in the case of BG correction. Apparently, the calibrations curves with and without BG correction should be similar only if the interval $p_a \pm \theta$ is higher than the line profile. Otherwise, the increase of concentration of the analyte or reduction of wavelength integration

interval would be accompanied by curving of the calibration curve. The issue is confirmed by the calibration graphs in Figure 8a obtained experimentally for Cu in the single element solutions using pixels 3, 4 and 5 from the line center for BG correction (curves 1-3, respectively). It is seen that the reduction of the integration interval due to BG correction is accompanied by sensitivity losses for higher concentrations of the analyte. In the Log-Log coordinates the curves are transformed into linear regressions *ax-b*. Respective graphs and approximations corresponding to the curves in Figure 8a are shown in Figure 8b together with correlation coefficients close to 0.999. It is seen from the figure that almost five orders of concentration magnitude constitute

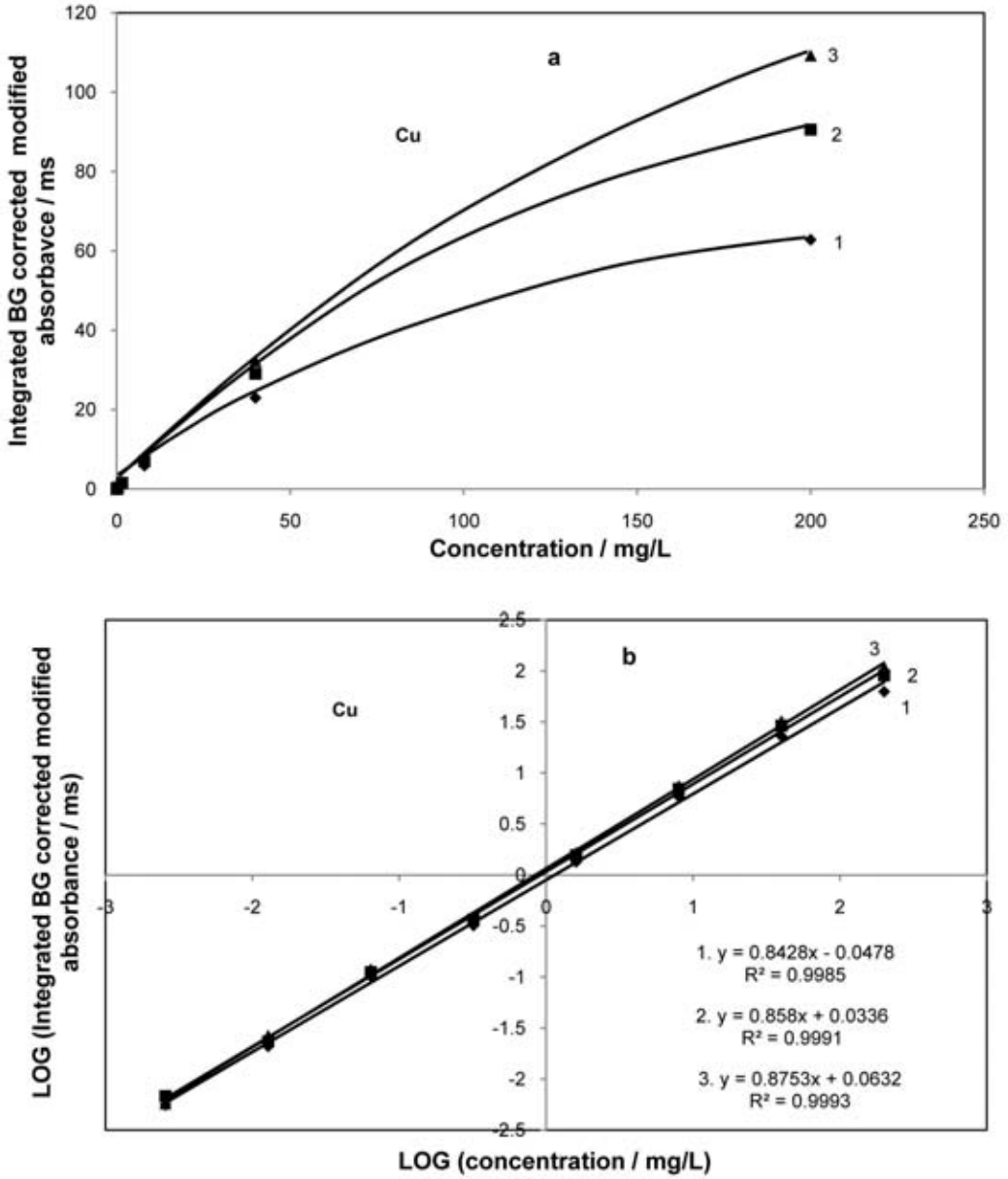

Figure 8. Calibration curves for Cu in the single element solutions in linear (a) and LOG-LOG (b) coordinates respectively: BG correction using average of the readings from third (1), fourth (2) and fifth (3) pixels from the line center.

the working range. For highest concentrations (200 mg/L) the data deviate from the linear approximation, especially for the smaller BG correction interval.

It can be pointed out that the deviations of BG corrected absorbance $\bar{A}$ (p_a,θ,i) from its true value $A(p_a,i)$ leading to the sensitivity reduction, are hardly important for practice if the vaporization kinetics is similar for the analyte in the sample and reference material. Otherwise, the deviations of parameter *a* from unity in the linear regression should cause determination errors. Those can be reduced if more distant from the line center pixels are employed for the BG correction. However, this method increases probability of spectral interferences associated with atomic lines. Thus, possibly, optimal parameter θ can be found for each spectral line and introduced in the calculation program. In this work, all calculations except those shown in Figure 8 were performed using a parameter θ equal to 3.

The approximations for the calibration curves for single element solutions and various lines are presented in Table 3. It is seen that the linearity range for most of the lines extends to about 3.5-4.5 orders of magnitude. For the regressions defined by correlation coefficient R^2>0.99 the slope of the graphs corresponds to parameter *a* between 0.92 and 0.99 for Al and Ca and mainly between 0.8 and 0.9 for other metals. These noted differences are not yet attributed to the properties of particular elements.

The Log-Log calibration graphs for the elements of Mixture 1, for the available concentrations below 0.5 mg/L overlap the graphs obtained independently using the solutions of individual elements, as it is shown in Figure 9, for the most sensitive lines of Al, Co, Fe, Cr and Mn. The graph for Cd in Mixture 1, constructed from the same as for other elements data matrix, has similar features to other elements in spite of not optimal for the element atomization temperature.

The upper concentration of the calibration curve depends on the sensitivity of the respective line. This is clearly indicated in Figure 9 by different deviations of the last data points (the data for 200 mg/L solutions) from the respective regression lines. The lowest linearity limit, 8 mg/L, was obtained for the most sensitive Mg 285.213 nm line.

4.5. Limit of detection

Limit of detection (LOD) for the elements was considered as the concentration that corresponded to integrated BG corrected modified absorbance equal to 3 standard deviations (SD) of blank measurements. The SD values were calculated from the data acquired in 10 blank measurements and respective LODs were evaluated using the calibration curves, Table 3. It is seen that for almost all elements the LOD found in this work for most sensitive lines are comparable or lower than LOD in Flame AAS in Table 1. Of note, the LODs can be still reduced on account of optimization of detection time for each element, multiple sample injection and selection of an optimal temperature program for the group of elements of similar volatility. Further reduction of LOD is also associated with the improvement of continuum light source and design of the atomizer.

4.6. Spectral interferences associated with superposition of atomic lines

The reduced resolution by the spectral instrument increases the probability of spectral interference due to overlap of the absorption lines of the analyte with the lines of other elements present in the sample. It is postulated that for elements of different volatility, mutual interferences can be reduced by optimization of the detection time and modification of temperature program. For analytes of similar volatility the contribution of spectral interferences in the measured absorbance can be evaluated by comparing the signals initiated by each of the individual analytes and other elements. In this work the evaluation was performed with the consideration that the sample includes Al, Fe, Co, Cu, Cr, Ni that have multi-line absorption spectra as well as Ca, Mg, K and Na, which are expected to be detected in natural ground water.

The concentrations of the analytes were taken as high as possible within the linear range of the calibration curves in Table 3 that provided maximum possible overlapping of the lines. Thus, the matrix of the temporary integrated BG

corrected absorption spectra for 40 mg/L solutions of individual elements (except 8mg/L for Mg) was composed. The approximations for the calibration curves in Table 3 made possible attribution of the output of particular pixels to the concentrations of the analyte. Thus, the contribution of interferences in the measured quantities could be evaluated.

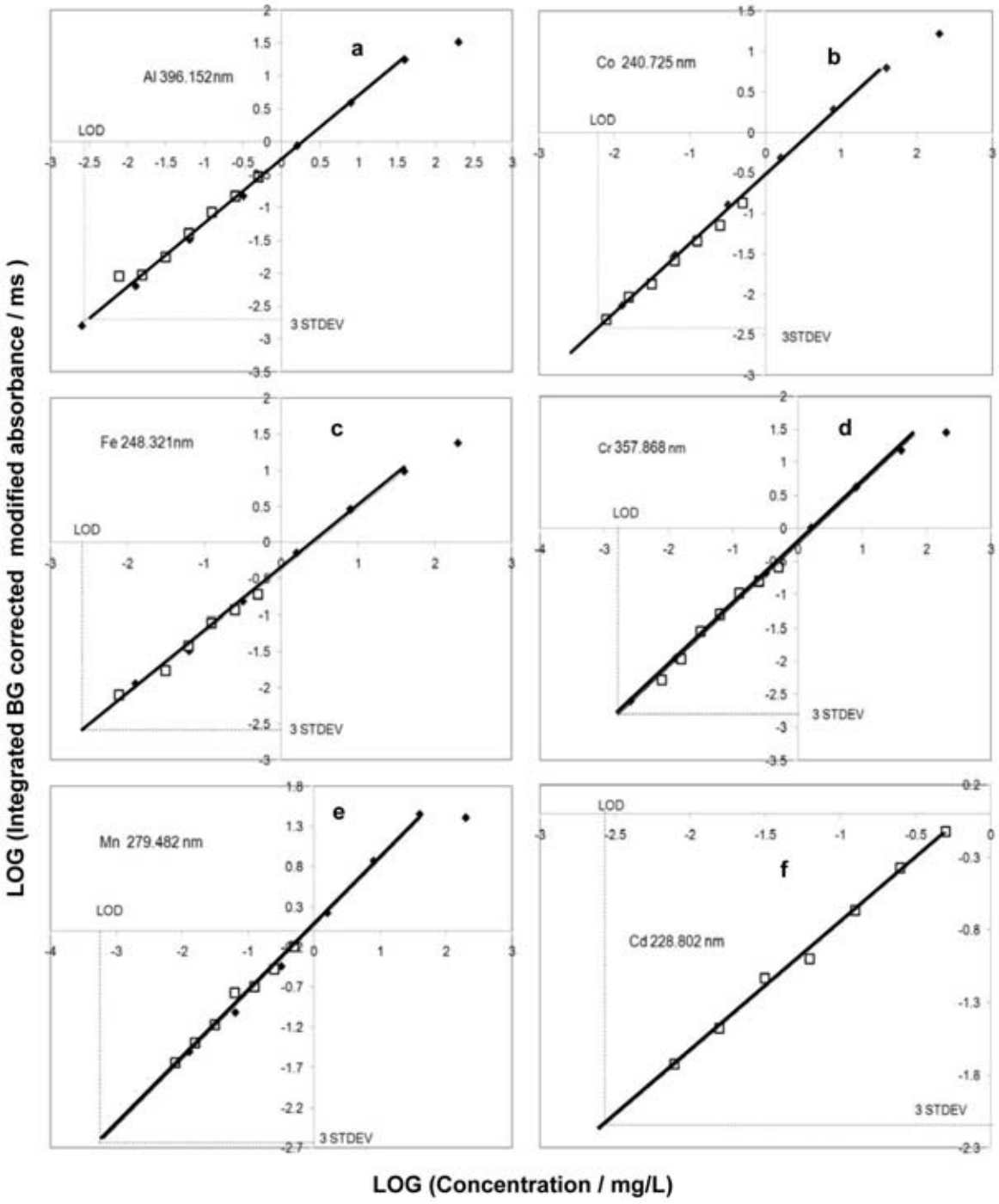

Figure 9. Calibration curves for the most sensitive lines of Al, Co, Fe, Cr, Mn, and Cd: for single element solutions (solid diamonds) and multi-element solutions obtained by dilution of Mixture 1 (empty squares).

Table 4. Concentrations attributed to the analyte and to the potential spectral interferences from other elements.

Element to determine	Wavelength /nm	The injected single element solution/concentration, mg/L[a]									
		Al/ 40	Ca/ 40	Co/ 40	Cr/ 40	Cu/ 40	Fe/ 40	Mg/ 8	Mn/ 40	Na / 40	Ni/ 40
		Concentrations evaluated using the approximations in Table 3									
Al	396.15	**39.87**	0.042	0.004	0.004	0.005	0.005	0.005	0.003	0.008	0.003
	394.40	**37.95**	0.023	0.011	0.002	0.014	0.005	0.016	0.004	0.007	0.013
	309.27	**40.29**	0.030	0.003	0.004	0.005	0.008	0.006	0.007	0.005	0.007
	308.22	**40.81**	0.097	2.32	0.069	0.064	0.083	0.075	0.070	0.047	0.382
	237.31	**37.40**	0.019	0.045	0.085	0.005	0.089	0.005	0.017	0.012	0.001
Ca	239.55	0.168	**42.97**	0.031	0.101	0.032	0.042	0.062	0.061	0.031	0.067
	227.55	0.420	**45.17**	0.447	0.135	0.076	0.398	0.062	0.106	0.076	0.203
Co	345.35	0.001	0.001	**37.89**	0.002	0.002	0.002	0.001	0.002	0.002	0.973
	340.51	0.013	0.021	**31.57**	0.026	0.004	0.022	0.006	0.018	0.024	0.012
	252.14	0.054	0.018	**41.93**	0.024	0.045	52.48	0.026	0.029	0.020	0.034
	242.49	0.002	0.005	**39.25**	0.001	0.001	0.002	0.001	0.003	0.002	0.103
	241.45	0.007	0.004	**42.53**	0.006	0.009	0.006	0.006	0.006	0.002	0.003
	241.16	0.000	0.002	**44.38**	0.000	0.002	0.007	0.005	0.009	0.002	0.057
	240.73	0.003	0.008	**41.31**	0.096	0.004	0.007	0.006	0.014	0.006	0.011
Cr	360.53	0.011	0.004	0.061	**40.63**	0.015	0.001	0.005	0.003	0.009	0.001
	359.35	0.013	0.011	0.486	**37.66**	0.007	0.007	0.007	0.008	0.009	0.003
	357.87	0.002	0.002	0.001	**35.68**	0.003	0.001	0.001	0.003	0.002	0.001
Cu	327.39	0.021	0.000	0.119	0.015	**41.96**	0.001	0.001	0.001	0.000	0.001
	324.75	0.023	0.001	0.117	0.017	**40.06**	0.002	0.002	0.001	0.002	0.021
Fe	302.06	0.016	0.003	0.001	0.412	0.004	**36.31**	0.002	0.002	0.004	0.020
	271.90	0.035	0.001	0.021	0.008	0.039	**43.52**	0.020	0.047	0.027	0.034
	252.29	0.024	0.010	31.04	0.001	0.020	**39.54**	0.010	0.012	0.008	0.016
	249.06	0.026	0.010	0.042	0.118	1.021	**37.61**	0.010	0.009	0.143	0.029
Fe	248.32	0.019	0.012	0.066	0.007	0.012	**36.81**	0.003	0.015	0.012	0.016
Mg	285.21	0.005	0.003	0.003	0.002	0.003	0.003	**7.26**	0.009	0.465	0.004
Mn	279.49	0.001	0.004	0.009	0.002	0.004	0.006	0.005	**37.15**	0.004	0.002
Na	330.24	0.341	0.032	0.027	0.027	0.015	0.017	0.017	0.030	**31.83**	0.058
	285.28	1.14	0.912	0.837	0.580	0.887	0.865	290.97	1.94	**36.97**	1.03
Ni	352.45	0.004	0.068	0.007	0.044	0.023	0.030	0.004	0.007	0.005	**43.68**
	341.48	0.025	0.068	3.05	0.041	0.047	0.008	0.008	0.010	0.018	**40.62**
	310.16	0.014	0.043	0.259	0.053	0.028	2.16	0.042	0.026	0.021	**36.98**
	305.08	0.015	0.061	0.024	0.009	0.049	0.004	0.041	0.042	0.021	**42.35**
	300.24	0.031	0.026	0.152	0.423	0.069	5.399	0.027	0.024	0.034	**40.31**
	232.00	0.019	0.082	0.083	0.075	0.051	0.555	0.020	0.016	0.019	**43.78**

[a]-The calculated values above 1mg/L are rounded to two decimal digits

The evaluation results are presented in Table 4. The concentrations of the analytes in the individual solutions found using the approximations for various lines, Table 3, are highlighted in each row. It is seen from the highlighted data that in general the difference between the true and calculated concentration remains within a 10-15% deviation range not exceeding 20%. In contrast, the spectra overlap for the majority of the lines causes an error less than 1%. The exceptions are indicated in Table 4 by the highlighted cells. The indicated data show that mutual interferences of Fe 252.29 and Co 252.14 or Mg 285.21 and Na 285.28 nm absorption lines do not permit using them for the determination if both components are present in the sample. Less significant error (from 5 to10%) is expected from interference of specific lines in Al, Co, Fe and Ni absorption spectra. Regardless, the list of interfering lines does not include the most sensitive ones and alternative lines can be utilized for determination of these elements.

5. Problems of SMET AAS application by the example of analysis of underground water

To delineate the strengths and weaknesses of the proposed methodology, it was applied to the simultaneous determination of elements in samples of borehole water. In order to highlight possible sources of errors the samples were not exposed to any chemical treatment or modification before or after injection into the atomizer. The temperature program detailed in Table 2, included relatively low pyrolysis temperature (600°C) that should prevent loss of the elements as volatile compounds before the atomization stage.

The calibration of the data was performed using the equations shown in Table 3. The determination results for 5 samples of borehole water are presented in Table 5. According to the analysis of potential spectral interferences, lines Fe 252.28, Co 252.13 and Mg 285.21, Na 285.28 were excluded from the data matrix. The data in each cell indicates the concentration calculated from the average of 3 measurements.

The results in Table 5 show that concentrations of some elements (e.g. Al and Fe) in various samples differ within 2-3 orders of magnitude. This broad range of concentrations makes simultaneous determination difficult without having reference calibration curves for the individual analytes. For the low concentrations, the output mainly correlates with LOD in Table 3 with low levels of spectral interference due to atomic lines. For high concentrations, the results obtained from multiple element lines typically demonstrate less than 20% deviation. However, greater deviations can be found, e.g. for Al 237.312 and Ca 239.55 nm lines in the BH4 sample. The source of the error is to be found from the visualization of the respective integrated or time resolved spectra.

To highlight the spectra features the injected volume of each sample was increased: 10 µl of liquid was injected in the tube five times; each sequential injection was performed after drying of previous portion and interruption of the temperature program after the drying step.

The selected time resolved spectra for the samples BH3 and BH4 are displayed in Figure 10 as example. The figures show that sample vapor beside main atomic constituents, Na, Mg, K, Ca, Ca, Si and in some cases Al and Fe, contains multiple molecular species, most part of which can be identified. The list of molecular constituents found in BH (1-5) samples includes AlCl [6, 20], AlF [6], MgCl [9, 10, 20], MgF [20], CS [6, 11, 21], SiO [6] and S_2, SO, SO_2 [11, 12]. For each sample a specific combination of atomic and molecular spectra is characteristic. Some of the bands appear simultaneously with atomic lines and, therefore, cannot be rid of by altering the temperature program.

The software makes possible to select and thoroughly investigate each particular part of the spectra. The example of such investigation is demonstrated by Figure 11 where the integrated spectra of samples BH3 and BH4 within 220-260 nm wavelength range are presented. It is evident that the deviations of the determination results for Al 237.312 and Ca 239.55 nm lines are caused by overlap with sharp SiO and AlF bands.

Easy visualization of the integrated or time resolved spectra helps in the optimization of temperature program or temporal interval in which atomic absorption of specific element

Table 5. Simultaneous determination of elements in the underground water.

Element	Wavelength / nm	Concentration / mg L^{-1}					LOQ[a]
		Borehole water sample					
		No 1	No 2	No 3	No 4	No 5	
Al	396.152	**0.058**[b]	0.003	*0.005*[c]	**4.894**	**0.046**	0.010
	394.401	**0.065**	0.004	*0.006*	**5.491**	**0.039**	0.015
	309.271	**0.110**	0.006	*0.008*	**5.637**	**0.087**	0.016
	308.215	**0.082**	0.008	*0.013*	**5.257**	**0.072**	0.039
	237.312	**0.083**	0.010	*0.021*	**8.825**	**0.052**	0.047
Ca	239.55	**2.342**	**5.117**	**11.304**	**1.050**	**16.604**	0.159
	227.546	**3.505**	**4.307**	**10.370**	**2.390**	**16.269**	0.105
Co	345.35	0.031	0.018	0.043	0.033	0.022	0.131
	340.512	0.027	0.018	0.027	0.026	0.031	0.124
	242.493	0.018	0.010	0.017	0.013	0.021	0.044
	240.725	0.011	0.008	0.009	0.011	0.026	0.028
Cr	360.532	0.009	0.003	0.002	*0.010*	0.004	0.014
	359.348	0.003	0.005	0.007	*0.014*	0.004	0.009
	357.868	0.006	0.004	0.002	*0.016*	0.003	0.009
Cu	327.39	**0.071**	0.009	**0.041**	**0.070**	**0.041**	0.009
	324.754	**0.069**	0.006	**0.037**	**0.055**	**0.040**	0.009
Fe	302.064	0.010	0.006	0.175	**2.593**	*0.021*	0.018
	271.903	0.035	0.004	0.171	**2.566**	*0.021*	0.197
	249.064	0.054	0.005	0.244	**2.904**	*0.059*	0.054
	248.321	0.014	0.007	0.133	**2.225**	*0.023*	0.020
Mn	279.482	0.004	0.004	**0.047**	**0.023**	0.004	0.007
Na	330.237	**14.133**	**12.365**	**6.628**	**4.309**	**10.626**	0.016
Ni	352.454	*0.064*	0.031	**0.155**	0.247	*0.076*	0.087
	341.476	*0.061*	0.032	**0.134**	0.041	*0.072*	0.094
	310.155	*0.078*	0.037	**0.120**	0.083	*0.074*	0.062
	305.082	*0.049*	0.046	**0.146**	0.053	*0.084*	0.255
	300.249	*0.072*	0.033	**0.108**	0.313	*0.046*	0.108
	232.003	*0.070*	0.055	**0.162**	0.170	*0.116*	0.120

[a]-Limit of quantification taken as 3LOD
[b]-Concentrations close or above LOQ indicated as bold figures
[c]-Concentrations close to LOD indicated as italics

should be detected to provide lower error along with an improved LOD. Instant observation of molecular spectra can also help for *in situ* chemical modification of the sample to reduce release of molecular species. In addition, molecular spectra collected with these techniques can be employed for the determination of sulfur or halogens.

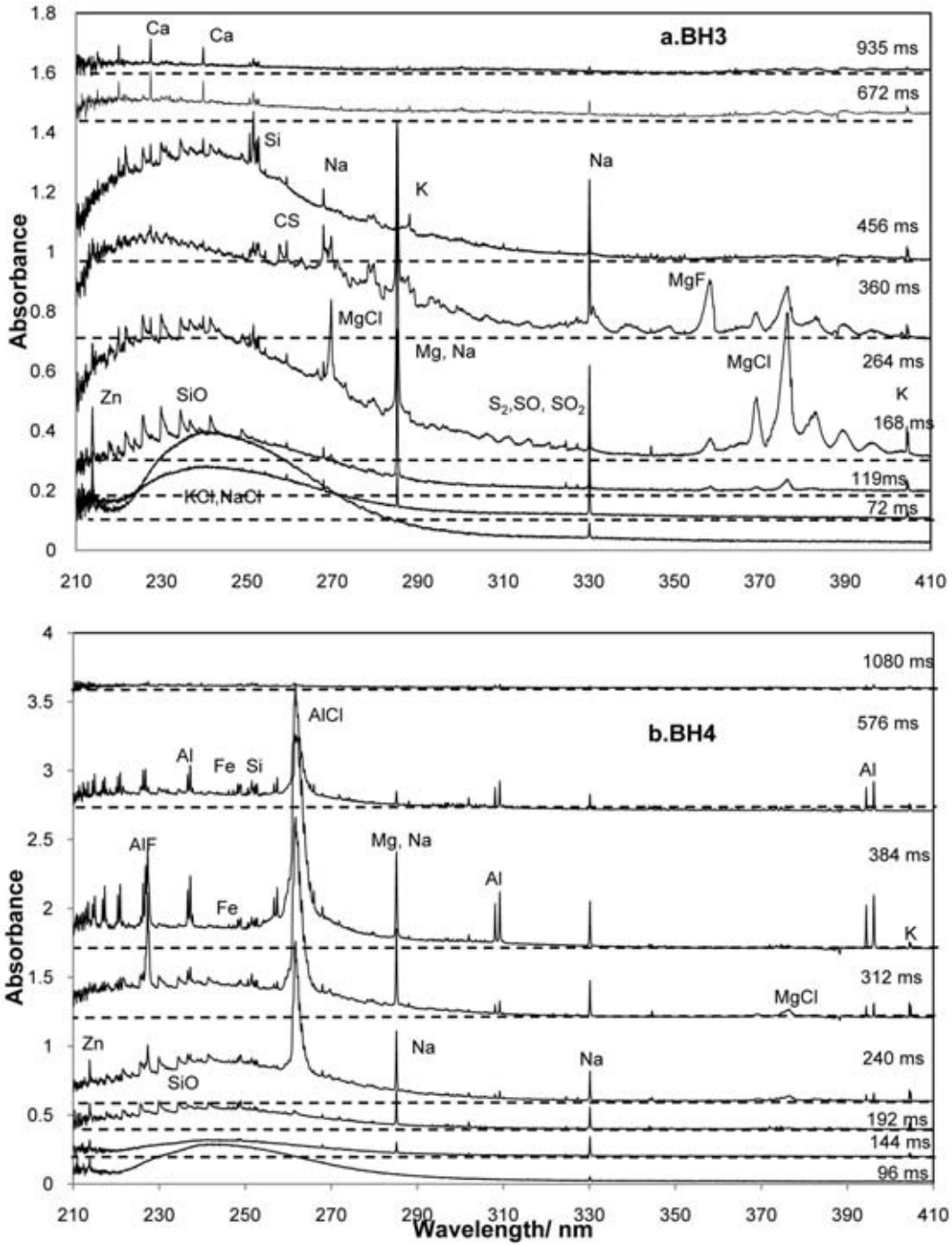

Figure 10. Selected absorption spectra indicating presence of molecular species in the vapor of the samples of underground water BH3 (a) and BH4 (b).

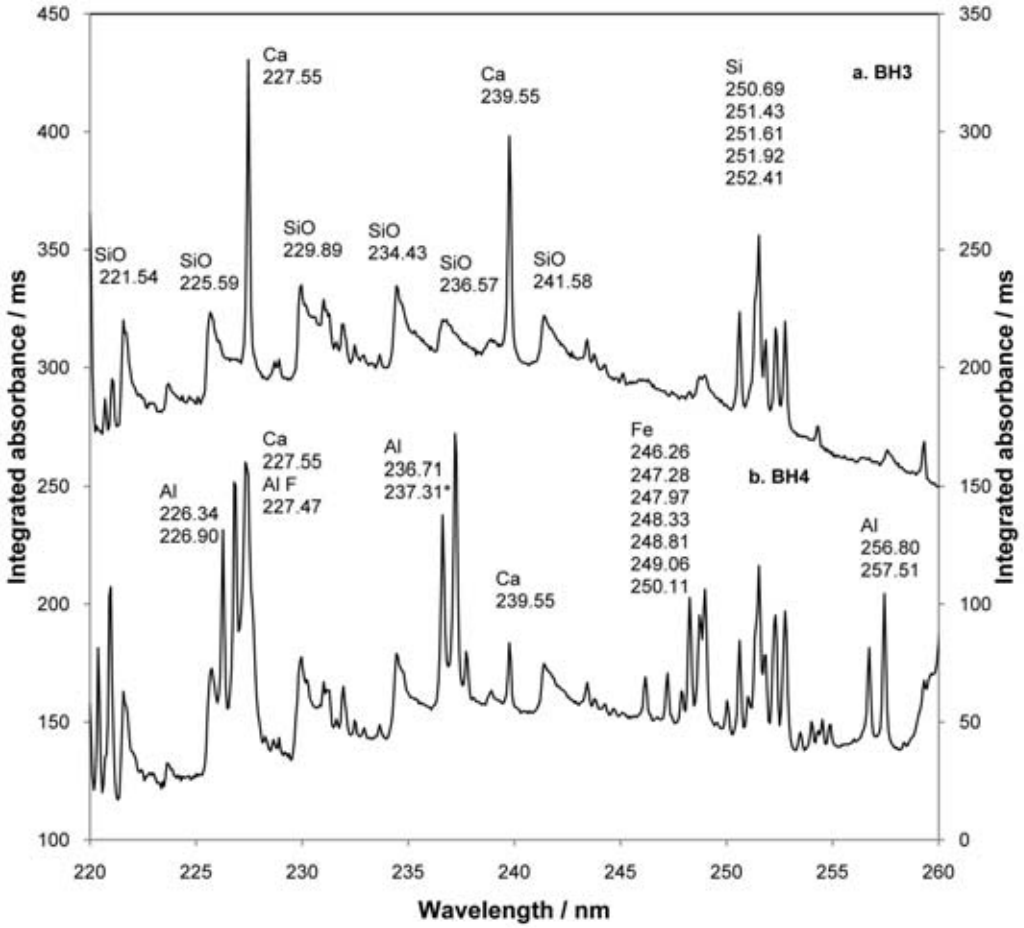

Figure 11. Identification of spectral bands for the underground water samples a-BH3 (secondary Y scale) and b-BH4 (primary Y scale).

CONCLUSION

Theoretical predictions provided the motivation for the instrument design and a prototype was built for an AA instrument containing coupling of a low resolution CCD spectrometer with continuum light source and a fast heated graphite tube atomizer. The instrument equipped with Xe arc lamp provides simultaneous determination of the elements suitable for pulse atomization in graphite tube atomizer with absorption lines between 210-410 nm. The working range for direct determination using single atomization pulse includes 4.5 orders of magnitude for concentrations above µg/L. The designed software provides BG correction, linearization of function absorption vs. concentration of atoms in the absorption volume and temporal integration of the modified absorption pulse. Visualization of absorption spectrum provides easy approach to the chemical modification of the sample, optimization of temperature program or use of molecular bands for analytical applications. The prototype instrument is user friendly, compact (bench top) and ergonomic. It can substitute for Flame AAS and importantly provides analytical advantages conferred by electrothermal atomization, fast spectra acquisition and data processing.

Further development of the theory and technique is required to provide the determination in the wavelength range from below 200 nm and increase sensitivity by modification of the atomizer and calculation algorithm. Acquisition of the molecular absorption spectra for a variety of analytes and samples will create a reference database for enhanced precision BG correction during multi-element determination.

ACKNOWLEDGEMENT

Author expressed gratitude to National Research Federation and Tshwane University of Technology, South Africa for the financial support.

REFERENCES

1. www.colloidalsciencelab.com/fact_pages/ Varian-MPX.pdf (accessed 14.08.2012).
2. Heitland, P. 2001, Spectro ICP Report, Nr ICP-32.
3. Boumans, P. W. J. M. (Ed.) 1987, Inductively Coupled Plasma Emission Spectroscopy - Part I, Methodology, Instrumentation and Performance, John Wiley & Sons, New York.
4. Lvov, B. V. 1970, Atomic Absorption Spectrochemical Analysis, Adam Hilger, London.
5. Welz, B. and Sperling, M. 1999, Atomic absorption spectrometry, 3rd Ed., WILEY-VCH, Weinheim.
6. Welz, B., Becker-Ross, H., Florek, S. and Heitmann, U. 2005, High-resolution continuum source AAS: The better way to do atomic absorption spectrometry, Wiley-VCH, Weinheim.
7. Katskov, D. A., Hlongwane, M., Heitmann, U. and Florek, S. 2012, Spectrochim. Acta Part B, 71-72, 14-23.
8. Katskov, D. A. and Khanye, G. E. 2010, S. Afr. J. Chem., 63, 45-57.
9. Daminelli, G., Katskov, D. A., Marais, P. J. J. G. and Tittarelli, P. 1998, Spectrochim. Acta Part B, 53, 945-964.
10. Daminelli, G., Katskov, D. A., Mofolo, R. M. and Kantor, T. 1999, Spectrochim. Acta Part B, 54, 683-697.
11. Katskov, D.A., Lemme, M. and Tittarelli, P. 2004, Spectrochim. Acta Part B, 59, 101-104.
12. Lemme, M., Katskov, D. A. and Tittarelli, P. 2004, Spectrochim. Acta Part B, 59, 115-124.
13. Katskov, D. A. and Sadagov Yu. 2011, Spectrochim. Acta, Part B, 66, 451-460.
14. Jim, G. and Katskov, D. 2011, S. Afr. J. Chem., 64, 71-78.
15. Tarasov, K. I. 1974, The Spectroscope, Adam Hilger, Bristole.
16. http://www.OceanOptics.com (accessed 14.08.2012).
17. http://www.hamamatsu.com (accessed 14.08.2012).
18. http://www.cortec.ru (accessed 14.08.2012).
19. Katskov, D. A., Shtepan, A. M., Grinshtein, I. L. and Pupyshev, A. A. 1992, Spectrochim. Acta Part B, 47, 1023-1041.
20. Plasus Specline Database (version 2.13), http://www.plasus.de
21. Jim, G., Katskov, D. and Tittarelli, P. 2011, Talanta, 5, 1687-1694.